Dimensional and geometrical precision of parts produced by Binder Jetting process as affected by the anisotropic shrinkage on sintering

Marco Zago[a], Nora Francesca Maria Lecis[b], Maurizio Vedani[b], Ilaria Cristofolini[a*]

[a] Department of Industrial Engineering, University of Trento, Via Sommarive 9, 38123 Trento - Italy

[b] Department of Mechanical Engineering, Politecnico di Milano, Via Privata Giuseppe La Masa 1, 20156 Milano – Italy

* Corresponding author: Ilaria Cristofolini, Department of Industrial Engineering, University of Trento, Via Sommarive 9, 38123 Trento – Italy
e-mail address: ilaria.cristofolini@unitn.it

Abstract

Dimensional and geometrical precision of parts produced by Binder Jetting is a crucial issue to be considered aiming at promoting the transition to industrial production. The influence of both the printing and the sintering processes has to be evaluated, and the high shrinkage has to be considered. The task is further complicated by the anisotropy of dimensional change on sintering.
The aim of this work is to investigate the dimensional and geometrical precision of cylindrical holes, as affected by the anisotropy of dimensional change on sintering after binder jetting. AISI 316L powder was used to produce five different geometries, characterized by four holes with different orientation with respect to the printing direction. The geometrical features were measured both in the green and in the sintered state with a coordinate measuring machine, and the dimensional changes, as well as the geometrical variations, were calculated. According to the author's previous experience, a theoretical model has been defined, which aims at predicting the geometry of the holes as derived by the anisotropic dimensional change on sintering. The expected dimensional change of hole diameters, the variation of cylindricity, and the variation of the axis inclination were calculated by the model and compared to those derived from measurement. Good agreement between predicted and measured results has been observed, providing that the influence of printing process parameters is considered.

Keywords: metal Additive Manufacturing, Binder Jetting, shrinkage on sintering, dimensional and geometrical precision

1. Introduction

Several additive manufacturing (AM) techniques have been developed during the last years, and seven different fabrication processes are listed in ASTM standard on the basis of the method used for adding material [1]. Binder jetting (BJ) looks promising for a future transition to industrial production due to the following characteristics: higher production rate at lower cost in comparison to powder bed fusion processes, virtually no limitation on material feedstock, high scalability, and a moderate investment cost on printing machine. In addition, BJ printing process does not require high energy consumption, neither controlled atmosphere in the printing area.

In BJ the as-built product needs to be further consolidated to provide the mechanical resistance. During the printing operation, the recoater spreads a layer of powder on the working plate, and the printhead selectively injects the binder agent on the corresponding CAD section. The green part obtained in this way is formed by weakly bonded particles, so the binder is cured to slightly enhance the green strength, before the extra powder is carefully removed. The part is then debinded by thermal or chemical treatment to obtain the so-called "brown part", which is sintered at high temperature to activate the diffusion mechanism strongly bonding the powders.

Recently, several studies investigated materials, process condition and design aspects aiming at improving the quality and performance of BJ products. Review papers effectively summarized the state of the art, and the most challenge parameters which influence the quality of the product [2–5]. The optimum particle size distribution has been studied [6–8], as well as the type and amount of binder providing the best quality of BJ products [9,10]. Nevertheless, BJ parts are obtained by a two-step process, and sintering plays a central role in determining the quality of parts, due to the high dimensional change on sintering, which could negatively influence the product accuracy when not considered in the design procedure [11,12]. Moreover, the dimensional change is anisotropic, and higher dimensional change in the printing direction than in the construction plane has been observed [7,13,14]. In some cases, shape distortion due to structure collapse during sintering has been highlighted [15,16].

Aiming at proposing effective design guidelines for additive manufacturing (DfAM), on the basis of the peculiar characteristics of the process, the dimensional and geometrical accuracy of the as-built product have been analyzed. Rebaioli et al. proposed an extensive review of the benchmarks geometry, to assess the dimensional and geometrical accuracy, the repeatability and minimum feature size of AM printing processes [17]. Vitolo et al. experimentally observed that flatness, circularity and cylindricity error increase on increasing sample size, and higher accuracy was reached in the samples positioned close to the printing starting point [18]. The form error determined by the staircase effect resulting from layer-by-layer building process has been also investigated. Arni and Gupta developed and successfully tested an algorithm for estimating the flatness error due to staircase effect [19]. Paul and Anand developed a theoretical model for assessing the cylindricity error induced by layer-by-layer fabrication and the approximation of the CAD shape by STL file [20]. The form error determined by polygon approximation of STL file is also examined on cylindrical holes by Ahn et al, who demonstrated that discrepancy converges close to zero in a finite number of polygon sides [21]. On the basis of the previous work, Paul and Anand investigated the optimal part orientation for minimizing the cylindricity and flatness form error, as well as the need for support structure of AM product [22]. Other studies investigated the form of cylindrical shape obtained by AM processes. Islam and Sacks observed a form error on multiple concentric cylinders, explained by the hypothesis of distortion of the layer during the printing process [23]. Ollison and Berisso analyzed the cylindricity on green samples which were fabricated by BJ process at different inclination angle [24], highlighting that inclination angle has a higher effect on form error than diameter size and printhead life. In another work, Farzadi et al examined the discrepancy between nominal and actual diameter of green parts printed along three different axis direction, observing a higher dimensional accuracy of samples aligned to X and Y fabrication directions with respect to Z direction [25].

A large amount of work, to date, experimentally investigated the accuracy of cylindrical parts, however, research mainly focused on the quality of as-built product. On the basis of author's previous experience [26–30], this work aims at studying the dimensional and geometrical error induced by the anisotropic dimensional variation on sintering on cylindrical holes, fabricated at different size and axis inclination. An analytical model has been proposed for assessing the diameter shrinkage, the circularity error, and the error of the inclination angle, as affected by the nominal dimension in the green state and by the anisotropic dimensional change in the fabrication reference system. The results of the model were compared with the experimental data, and good agreement between predicted and measured data was found.

2. Material and Methods

Figure 1 shows the geometry of the samples produced by binder jetting in order to study the dimensional and geometrical precision of the holes in the green and sintered state. The nominal diameters of the through holes are 3, 5, 7, and 9 mm, and the inter-axes, as well as the position in the plane orthogonal to the axes, were nominally the same in all the samples. The dimensions of the plane orthogonal to the axes of the holes were also kept nominally the same in all the samples, 70 mm x 20 mm, while the inclination with respect to the building plane was different, varying from 0° to 90°, as shown in Figure 1.

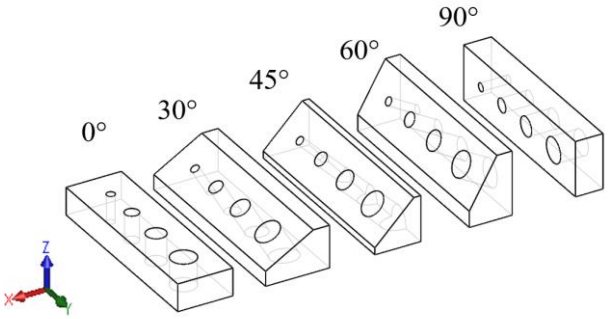

Figure 1. The geometry of the test samples.

The main features to be referred in the following are shown in the section view in Figure 2, and listed in Table 1.

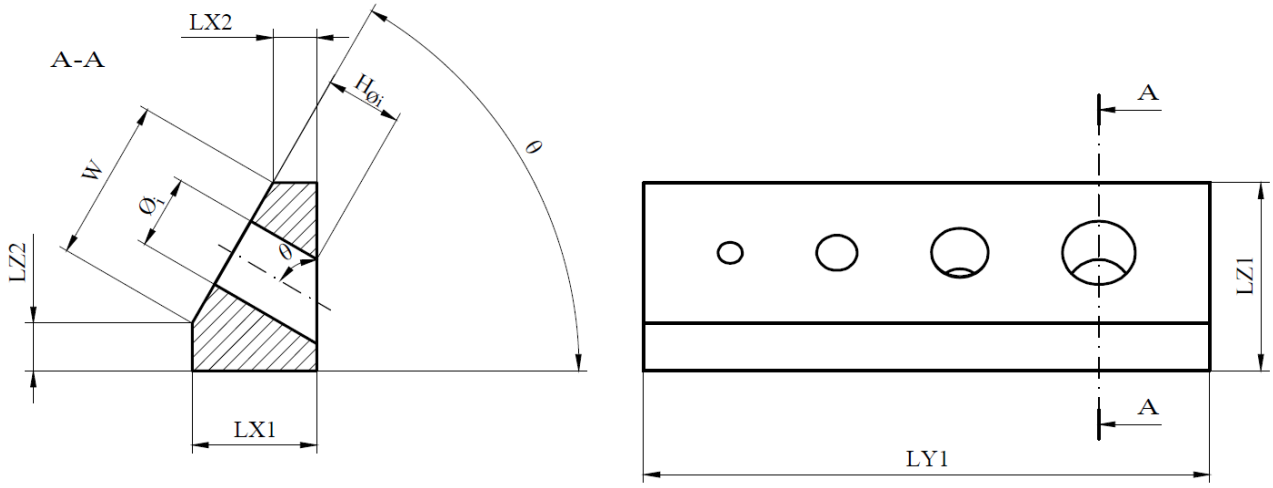

Figure 2. Section view and conventional name of the main features in inclined samples.

Table 1. Nominal dimensions of the samples (all dimensions are in millimeters).

Sample	LX1	LX2	LY1	LZ1	LZ2	ϕ3	ϕ5	ϕ7	ϕ9	Hϕ3	Hϕ5	Hϕ7	Hϕ9	W
0°	20	-	70	10	-	3	5	7	9	10	10	10	10	-
30°	23.191	5.871	70	15.410	5.41	3	5	7	9	11.155	10.577	10	9.423	20
45°	16.617	2.475	70	16.617	2.475	3	5	7	9	12	11	10	9	20
60°	15.41	5.41	70	23.191	5.871	3	5	7	9	11.155	10.577	10	9.423	20
90°	10	-	70	20	-	3	5	7	9	10	10	10	10	-

Samples have been designed aiming at obtaining the highest comparability among the data, and the geometry of the different samples has been defined on the basis of the effective depth of the holes (Hϕi), which corresponds to a complete cylindrical hole in inclined samples. Specifically, the hole with 7 mm diameter has been taken as reference, imposing its effective depth nominally equal to 10 mm for all the samples, as by Table 1. Providing that the surface orthogonal to the axes of the holes is the same for all the samples (70 mm x 20 mm, as previously stated), the remaining dimensions of the samples have been defined on the basis of the reference hole, as by equations (1), (2), and (3), whose terms are identified in Figure 2 and Table 1, for samples inclined 45° and 60°. For sample inclined 30° equations are the same, providing that the complementary angle is considered instead of (θ) and labels X and Z are permuted.

$$LX1 = \left(\frac{\phi_7}{2} + \frac{W}{2}\right)\cos\theta + H_{\phi 7}\sin\theta \qquad (1)$$

$$LX2 = \left(\frac{\phi_7}{2} - \frac{W}{2}\right)\cos\theta + H_{\phi 7}\sin\theta \quad (2)$$

$$LZ1 = LZ2 + W\cos\theta \quad (3)$$

In this way the effective depth is very close to 10 mm for all the holes in any configuration, which is important in defining homogeneous measurement procedure. Moreover, in this way the diameter shrinkage and cylindricity variation only depend on diameter and inclination.

Samples were built using gas atomized AISI 316L stainless steel powder, featuring a particle size distribution D90 (25 μm), D50 (10 μm), D10 (4 μm), according to the powder supplier. The use of AISI 316L in binder jetting has been extensively studied [5], and it is currently considered as a reference material for the BJ processing. A group of five different geometries was printed in a single batch using ExOne Innovent+ system machine. Two other batches were printed later in order to obtain three replicates for each geometry. In each printing operation, samples were located in the same position in the building chamber, and all the production process parameters were kept the same, reducing as much as possible the process variability. As shown in Figure 1, the largest dimensions were built up parallel to Y direction, which corresponds to the movement direction of the printing head, while smaller dimensions in the printing plane were oriented parallel to X axis, which corresponds to the movement direction of the recoater, so that any influence of printing direction would affect all the samples in the same way. The process parameters summarized in Table 2 have been identified in a previous work [31], as the best combination for controlling the dimensional stability of green parts.

Table 2. BJ process parameters used for the production of the investigated samples.

Printing					**Curing**	
Layer thickness	**Saturation level**	**recoat (mm/s)**	**Roller (rpm)**	**Ultrasonic intensity**	**Temperature**	**Time (min)**
50 μm	55%	90	500	100%	180°C	180

Samples were measured in the green and sintered state using a Coordinate Measuring Machine (CMM) Global DEA 07-07-07 equipped with a Renishaw SP600M scanning head - contact probe 1 mm tip. Clamping configuration is shown in Figure 3, providing good accessibility to all the features to be measured.

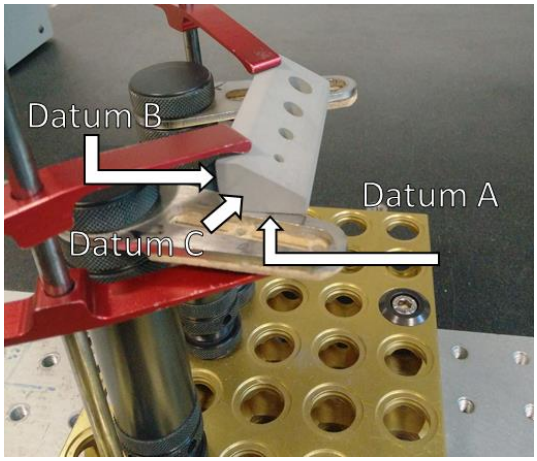

Figure 3. Clamping configuration adopted for the measurement of green and sintered samples, along with the planes defining the datum reference system in the alignment procedure.

A specific measurement routine was programmed for each geometry in Hexagon Pc-Dmis 2019R2 software suite, consisting in manual alignment, which approximately identifies the position of the samples with respect to the CMM reference system. The final alignment was obtained measuring specific points identified in the CAD model. In the alignment, the primary datum plane A corresponds to the first layer built in the printing process, while secondary (B) and tertiary (C) datum planes correspond to the features indicated in Figure 3. The planes were obtained by points measured in "point by point" mode, aiming at avoiding any damage likely occurring in green parts in continuous scan. 50 to 150 points were acquired for each plane depending on the surface area, as shown in Figure 4. Planes were reconstructed by least squares method and the linear dimensions (LX1, LY1, LZ1) were calculated as distances between planes. Dimension LZ2 was calculated as the distance between datum plane A and the straight line obtained by the intersection of the inclined plane and the plane corresponding to LZ2. The same approach was used to calculate dimension LX2.

The effective depth of the holes $H_{\phi i}$ was estimated by equation (1), considering the measured values of angle θ and linear dimensions (W, LX1), and the nominal diameter of the hole in place of ϕ_7. The surface of the holes was reconstructed through five circles, measured at equidistant levels; each circle was derived from 12 equidistant points measured at given distance from the plane orthogonal to the axes. Both circles and cylindrical surface were derived by least squares method. For each hole the diameter corresponded to the diameter of the derived cylindrical surface. Considering form characteristics, cylindricity was derived evaluating the two coaxial cylindrical surfaces containing all the measured points on the surface of holes, according to [32].

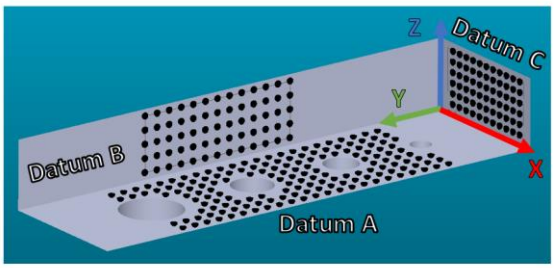

Figure 4. Points selected in the CAD model and further acquired in order to define the datum planes A, B and C, on sample 0°.

After measurement, green parts were debinded in Ar atmosphere at 470°C for 4 hours and sintered for 3 hours in a vacuum furnace (HT-S1 LPC by HTS, Mozzanica BG, Italy) at a pressure of 10^{-1} mbar, and temperature of 1360°C, reached with a heating rate of 5 °C/min. During sintering the samples were placed on alumina holders to avoid contamination from the molybdenum plate of the furnace.

The measurement procedure above described was repeated to measure the sintered parts, slightly modifying the position and the number of the points to be acquired, due to the large shrinkage occurred on sintering, which determined significant differences with respect to the CAD model of green parts. The dimensional changes of linear dimensions (ε_L) and diameters (ε_ϕ) were computed by equations (4) and (5), respectively.

$$\varepsilon_L = \frac{Li_s - Li_g}{Li_g} \tag{4}$$

$$\varepsilon_\phi = \frac{\phi_s - \phi_g}{\phi_g} \tag{5}$$

Where the subscripts g and s correspond to the green and sintering state, respectively.

2.1 Theoretical model

Focusing the attention on the anisotropic shrinkage on sintering, with respect to the reference system in the printing area, a model has been developed to estimate the dimensional and geometrical changes. This model describes the cylindrical holes of the investigated samples and aims at predicting the dimensional change of diameter and inclination angle, and the variation of circularity as function of both the nominal diameter and the axis inclination in the green state. Some analytical relationships are proposed and the numerical solution is compared to the experimental data in the *Results and discussion* section.

In Figure 5, the generic cylindrical shape, whose axis is inclined with respect to the reference system in the printing area XYZ, is usefully described through a second reference system X'Y'Z', where Y' and Y are overlapped, and both X' and Z' are rotated counterclockwise by an angle θ around Y' axis. In the X'Y'Z' reference system, the axis of the hole corresponds to Z' direction, and the circular section belongs to plane X'Y'. The points belonging to the circular sections are defined by cylindrical coordinates (r, α, Z').

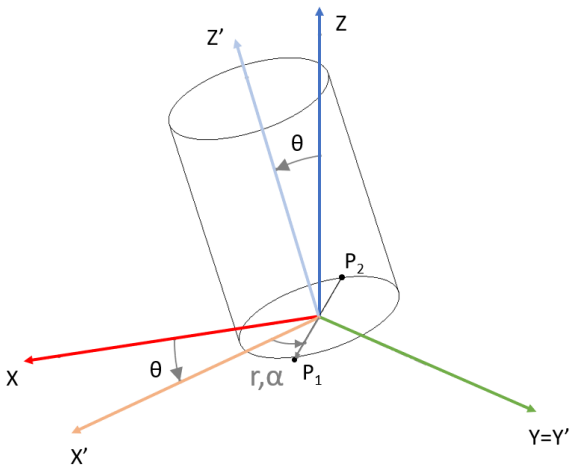

Figure 5. Schematic representation of: the reference system in the printing area (XYZ), the reference system rotated by θ angle with respect to Y' (X'Y'Z'), and the reference system in cylindrical coordinates (r,α,Z').

Aiming at predicting the dimensional change on sintering of the diameter, two opposite points (P1 and P2 in Figure 5) belonging to X'Y' plane, at a given Z' coordinate, are considered. These points in the X'Y'Z' reference system can be expressed by equations (6) and (7) in cylindrical coordinates.

$$\begin{Bmatrix} x'_{P1} \\ y'_{P1} \\ z'_{P1} \end{Bmatrix} = \begin{Bmatrix} r\cos\alpha \\ r\sin\alpha \\ z'_0 \end{Bmatrix} \tag{6}$$

$$\begin{Bmatrix} x'_{P2} \\ y'_{P2} \\ z'_{P2} \end{Bmatrix} = \begin{Bmatrix} r\cos(\alpha+\pi) \\ r\sin(\alpha+\pi) \\ z'_0 \end{Bmatrix} = \begin{Bmatrix} -r\cos\alpha \\ -r\sin\alpha \\ z'_0 \end{Bmatrix} \tag{7}$$

Using the two opposite points P1 and P2, the diameter in the green (ϕ'_g) and sintered (ϕ'_s) state can be expressed by equations (8) and (9), respectively.

$$\phi'_g = \sqrt{\left(x'_{g-P2} - x'_{g-P1}\right)^2 + \left(y'_{g-P2} - y'_{g-P1}\right)^2 + \left(z'_{g-P2} - z'_{g-P1}\right)^2} \tag{8}$$

$$\phi'_s = \sqrt{(x'_{s-P2} - x'_{s-P1})^2 + (y'_{s-P2} - y'_{s-P1})^2 + (z'_{s-P2} - z'_{s-P1})^2} \tag{9}$$

Therefore, the dimensional change of the diameter in X'Y'Z' reference system ($\varepsilon'_{\phi i}$) can be computed by equation (10).

$$\varepsilon'_{\phi i} = \frac{\phi'_s - \phi'_g}{\phi'_g} \tag{10}$$

In the XYZ reference system the linear dimensional changes on sintering are ε_x, ε_y, and ε_z, which are calculated by equation (4) considering the linear dimensions in X, Y, and Z directions. Consequently, the relationships between the points in the green and sintered state can be expressed by equation (11).

$$\begin{Bmatrix} x_{s-i} \\ y_{s-i} \\ z_{s-i} \end{Bmatrix} = \begin{bmatrix} 1+\varepsilon_x & 0 & 0 \\ 0 & 1+\varepsilon_y & 0 \\ 0 & 0 & 1+\varepsilon_z \end{bmatrix} \begin{Bmatrix} x_{g-i} \\ x_{g-i} \\ x_{g-i} \end{Bmatrix} \tag{11}$$

Where subscript *i* identifies each specific point.

In order to rotate the points from XYZ to X'Y'Z' reference system, and vice versa from X'Y'Z' to XYZ, the rotational matrix is introduced by equations (12) and (13), respectively

$$\begin{Bmatrix} x_{g-i} \\ y_{g-i} \\ z_{g-i} \end{Bmatrix} = \begin{bmatrix} \cos\theta_g & 0 & -\sin\theta_g \\ 0 & 1 & 0 \\ \sin\theta_g & 0 & \cos\theta_g \end{bmatrix} \begin{Bmatrix} x'_{g-i} \\ y'_{g-i} \\ z'_{g-i} \end{Bmatrix} \tag{12}$$

$$\begin{Bmatrix} x'_{s-i} \\ y'_{s-i} \\ z'_{s-i} \end{Bmatrix} = \begin{bmatrix} \cos\theta_s & 0 & \sin\theta_s \\ 0 & 1 & 0 \\ -\sin\theta_s & 0 & \cos\theta_s \end{bmatrix} \begin{Bmatrix} x_{s-i} \\ y_{s-i} \\ z_{s-i} \end{Bmatrix} \tag{13}$$

where θ_g and θ_s correspond to the angle between cylinder axis and building direction in the green and sintered state, respectively. The anisotropic dimensional change on sintering determines a variation of the inclination angle θ, which can be calculated by equation (14).

$$\theta_s = \tan^{-1}\left(\frac{x_s}{z_s}\right) = \tan^{-1}\left[\tan\theta_g \frac{(\varepsilon_x + 1)}{(\varepsilon_z + 1)}\right] \tag{14}$$

Using equations (6-9) and (11-13) to determine the terms in equation (10), the dimensional change of the diameter defined by the two opposite points can be expressed by equation (15) as a function of:

- the dimensional changes ε_x, ε_y and ε_z in the printing area reference system;
- the angle θ_g between the cylinder axis and the reference system in the printing area at the green state;
- the angle α, corresponding to the points of the circular sections in cylindrical coordinates.

$$\varepsilon'_{\phi i} = \sqrt{\cos^2\alpha\left[(\varepsilon_x + 1)^2\cos^2\theta_g + (\varepsilon_z + 1)^2\sin^2\theta_g\right] + \sin^2\alpha\left(\varepsilon_y + 1\right)^2} - 1 \tag{15}$$

Along X' and Y' axis (α= 0° and α=90°, respectively), equation (15) can be simplified in equations (16) and (17).

$$\varepsilon'_x = \sqrt{\left[(\varepsilon_x + 1)^2 \cos^2 \theta_g + (\varepsilon_z + 1)^2 \sin^2 \theta_g\right]} - 1 \tag{16}$$

$$\varepsilon'_y = \varepsilon_y \tag{17}$$

Figure 6 reports the graphical solution of equation (15) as a function of θ_g (calculated for different α values).

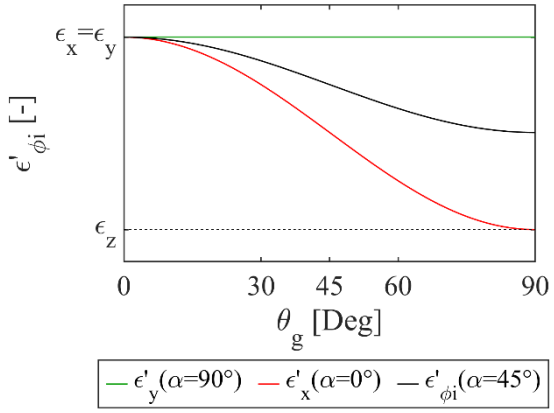

Figure 6. Dimensional change of diameter defined by two opposite points (as by equation (15)) versus the inclination angle of the axis θ_g.

The curves in Figure 6 demonstrate that $\varepsilon'_{\phi i}$ depends on α angle. This means that, inclining the axis of the hole, the section of the cylinder evolves from a circular shape, in the green state, to an elliptical profile, in the sintered state, as confirmed by the different dimensional changes ε'_x and ε'_y. In order to validate the theoretical model, the measured dimensional change of diameter and the variation in cylindricity are compared to the predicted ones.

Two alternative approaches were studied for assessing the dimensional change of the diameter. The first approach is based on an algorithm, while the second one on an analytical approximation. In both methods, the starting point of the model is represented by the nominal shape and dimensions in the green state. According to the first approach, a dataset of points belonging to the circle defined by the nominal diameter was expressed in cylindrical coordinates by equation (6) at different α angle position. The points were then rotated from X'Y'Z' to XYZ reference system by equation (12). Due to the anisotropic dimensional change on sintering, the points are expected to move to the coordinates calculated by equation (11), and the resulting points were fitted by least squares method in order to obtain the estimation of the hole diameter in the sintered state. According to this procedure, the theoretical dimensional change of diameter ($\varepsilon_{\phi-best\ fit}$) can be predicted by the model through equation (10), and compared with the measured dimensional change given by equation (5).

This method allows a proper comparison between predicted and measured data, but it is based on an algorithm which provides a non-linear problem, so that only numerical solutions can be determined.

In order to estimate an alternative analytical approach, the average dimensional change of the diameter ($\varepsilon_{\phi-average}$) has been evaluated by equation (18), which averages the dimensional change defined by equation (15) along α angle

$$\varepsilon_{\phi-average} = \frac{\int_0^{2\pi} \varepsilon'_{\phi i}\, d\alpha}{2\pi} \tag{18}$$

Defining $\left(\varepsilon_y + 1\right)^2 = B$ and $\left[(\varepsilon_x + 1)^2 \cos^2\theta_g + (\varepsilon_z + 1)^2 \sin^2\theta_g\right] = A$, equation (18) turns to equation (19), incorporating an elliptic integral, whose close form solution is not available. Nevertheless, this approach allows an easier estimation of the dimensional change of diameter, modelling the elliptical section by aligning minor and major axis with X' and Y' directions, respectively.

$$\varepsilon_{\phi-average} = \frac{\sqrt{A}}{2\pi}\int_0^{2\pi} \sqrt{1 - \frac{(A-B)}{A}\sin^2\alpha}\, d\alpha - 1 \tag{19}$$

Table 3 reports the dimensional change of the diameter calculated by least squares method and by average method supposing ε_x and ε_y equal to -15% and ε_z equal to -18%, according to the experimental data of this study. The results reveal a marginal discrepancy between the two estimation methods, which demonstrates that equation (19) can effectively predict the dimensional change of the cylindrical hole accounting for the anisotropic dimensional change.

Table 3. Example of the numerical solution and discrepancy of the dimensional change of diameter calculated by average and best fit methods at different θ_g angles.

$\boldsymbol{\theta_g}$ **[Deg]**	$\boldsymbol{\varepsilon_{\phi-best\,fit}}$ **[%]**	$\boldsymbol{\varepsilon_{\phi-average}}$ **[%]**	$\boldsymbol{\varepsilon_{\phi-best\,fit} - \varepsilon_{\phi-average}}$ **[%]**
0°	-15	-15	0
30°	-15.367	-15.370	0.002
45°	-15.733	-15.742	0.009
60°	-16.096	-16.116	0.020
90°	-16.458	-16.493	0.035

As mentioned earlier, due to the anisotropic dimensional change the circular section of the hole in the green state turns to an elliptical section in the sintered state, which can be estimated by circularity error. Circularity error can be evaluated by equation (20), which computes the difference between the major and minor axes of the resulting ellipse in the sintered state.

$$circularity\ error = \frac{\phi'_s(\alpha = 90°) - \phi'_s(\alpha = 0°)}{2} \tag{20}$$

The major and minor axes of the ellipse can be compared to the green diameter and the dimensional change is defined by equations (21) and (22).

$$\phi'_s(\alpha = 90°) = \left(\varepsilon'_y + 1\right)\phi'_g \tag{21}$$

$$\phi'_s(\alpha = 0°) = (\varepsilon'_x + 1)\phi'_g \tag{22}$$

Replacing equations (21) and (22) in equation (20), and subsequently equations (16) and (17), the circularity error can be expressed by equation (23) as a function of:

- the diameter in the green state ϕ'_g;
- the dimensional changes ε_x, ε_y and ε_z;

- the angle θ_g between the cylinder axis and the reference system in the printing area at the green state.

$$circularity\ error = \frac{1}{2}\phi'_g\left\{(\varepsilon_y + 1) - \sqrt{\left[(\varepsilon_x + 1)^2 \cos^2\theta_g + (\varepsilon_z + 1)^2 \sin^2\theta_g\right]}\right\} \quad (23)$$

In conclusion, this theoretical model proposes an analytical description for: the local and average dimensional change of diameter, the dimensional change of the inclination angle, and the variation of circularity as function of the geometrical parameters of the cylinders representing the holes. The dimensional change of diameter, and consequently the variation in circularity, as derived from equation (15), do not depend on the coordinate Z', so that they describe the whole cylinder. The circularity can be referred to different levels in the hole, and the resulting envelope might express the cylindricity of the hole. The model, in fact, focuses on the anisotropic shrinkage on sintering with respect to the printed reference system, which is considered as prevailing with respect to other variables, for example staircase effect, or gravity force influence. The influence of these parameters, which might determine further variation of dimensions and shape along the axis of the holes, is expected to be less significant, and it might be considered in further refinement of the model.

3. Results and discussion

Dimensional changes of linear dimensions (linear shrinkage), diameters and geometrical parameters of the holes (cylindricity and inclination of the axis), are presented in the following sections, as derived from measurement, and are compared to the expected values resulting from the analytical model.

3.1 Linear shrinkage

Figure 7 illustrates the linear shrinkage of dimensions LX1, LX2, LY1, LZ1 and LZ2 versus the nominal size for all the samples. This plot clearly evidences the higher shrinkage along Z direction, while almost isotropic behavior on X-Y plane can be reasonably derived, despite only one nominal dimension was investigated along Y direction.

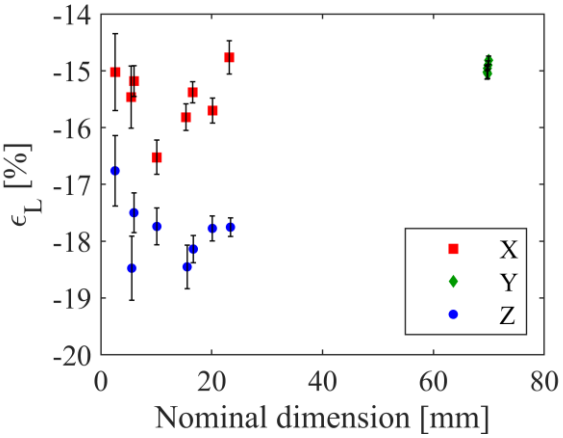

Figure 7. Linear shrinkage of dimensions: LX1, LX2, LY1, LZ1, LZ2 of the five geometries versus the nominal sizes (see Table 1). The error bars represent one standard deviation in the measurements.

The anisotropic shrinkage on sintering of AISI 316L stainless steel in BJ process is reported in literature [5,33], however, the different explanations generally refer to sintering process, not specifically dealing with sintering after BJ. The influence of gravity on the higher shrinkage along Z axis is suggested by some authors [7,13]. Olevsky and German proposed a sintering model which incorporates gravity force and surface transport mechanisms for predicting anisotropic dimensional change of cylindrical samples [34]. A

further work investigates the shape distortion of a cylinder by finite element method, incorporating the viscous material constitutive law and gravity effect [35]. The synergistic effect of gravity force and sintering mechanisms is supposed to determine the anisotropic shrinkage, and to deform the cylindrical shape in a truncate cone (elephant foot effect). Nevertheless, the mechanism above strongly depends on the investigated material and sintering conditions, and can be hardly considered in the conditions of the present study. In fact, in Rishmawi et al, cylindrical samples were produced by BJ from water-atomized iron powder. No shape deformation was observed while the measured dimensional change did not reveal an evident discrepancy between top and bottom circles [36]. Similarly, in the present work the dimensional change of LX1 and LX2 are practically the same in all the samples, providing that the way they are derived is considered, as explained in the following. Therefore, gravity might have determined the higher dimensional change along Z direction but the dimensional change in X-Y plane is not affected by sample height as proposed by Olevsky and German. Further experimental analysis should clarify the origin of anisotropic dimensional change in order to establish the physical principles governing the phenomenon.

As noted in Figure 7, the data corresponding to the smaller nominal dimensions are quite scattered, and the scatter band corresponding to smaller nominal dimensions is larger, but this is likely due to the way they have been derived. As previously stated, LZ2 and LX2 cannot be derived as distances between planes, and the dimensional changes can be affected consequently. Nevertheless, considering the dimensional changes related to distances derived by planes, negligible influence of the nominal dimension can be observed. Table 4 reports the mean value and the standard deviation of the linear dimensional changes. The shrinkages along X and Y directions are very close. Further analysis should enlarge the interval of dimensions investigated in order to prove the independence of linear shrinkage from nominal geometry.

Table 4. Mean value and standard deviation of the linear shrinkage of the five geometries grouped along the workspace reference system.

Printing direction	**Mean ε_L [%]**	**Std. Dev.ε_L [%]**
X	-15.5%	0.8
Y	-14.9%	0.2
Z	-17.8%	0.8

3.2 Dimensional change of diameters

The dimensional change of diameters was computed by equation (5), and the experimental results are reported in Figure 8, along with the values predicted by the theoretical model. From here on, the error bars represent one standard deviation in the measurements.

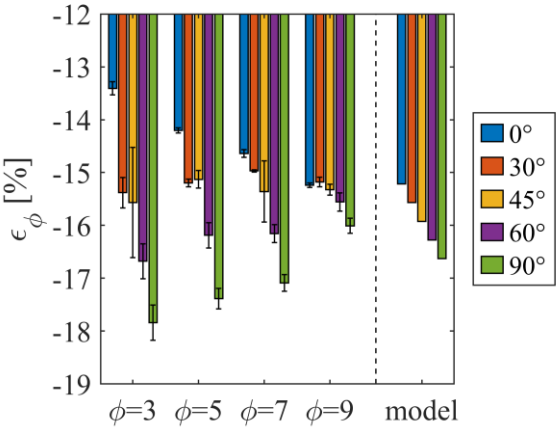

Figure 8. Measured and predicted dimensional change on sintering of the different holes at angle θ_g between the cylinder axis and the reference system in the printing area - green state

Experimental data in Figure 8 show that diameter shrinkage tendentially increases on increasing the inclination angle of the axis of the hole, according to the trend predicted by the theoretical model considering the anisotropic shrinkage. The data related to the theoretical model in Figure 8 have been derived from equation (19) using the mean dimensional changes reported in Table 4 to calculate the equation parameters. Nevertheless, experimental data are also affected by the nominal diameter size. Table 5 reports the normalized difference (Δ) between the predicted diameter shrinkage ($\varepsilon'_{\phi-average}$) and the experimental one, as calculated by equation (24).

$$\Delta = \frac{\varepsilon'_{\phi-average} - \varepsilon_{\phi}}{\varepsilon_{\phi}} \quad (24)$$

Table 5. Difference between predicted and measured dimensional change on sintering in diameter for different sizes and inclinations of holes – mean values are considered.

	Δ				
Nominal diameter / **Inclination angle**	0°	30°	45°	60°	90°
ϕ3	13.5%	1.2%	2.3%	-2.4%	-6.8%
ϕ5	7.1%	2.4%	5.2%	0.5%	-4.3%
ϕ7	3.9%	4.0%	3.7%	0.7%	-2.7%
ϕ9	-0.2%	2.6%	3.9%	4.6%	3.9%

Considering the data provided in Figure 8 and Table 5, it can be observed that the dimensional change of diameter is generally overestimated by the theoretical model, and the largest differences are observed in the smallest holes. The shrinking phenomena occurring on sintering, which might be influenced by the size, could be related the gravity force and/or to inhomogeneous heating rate during the sintering process, not considered in the theoretical model.

The influence of gravity force on diameter shrinkage can be highlighted considering samples 90°, and related to the underestimation of the dimensional change by the theoretical model. In Figure 8 (green bars), the dimensional change of diameter significantly increases on decreasing the diameter size, likely due to the corresponding increased mass of material above the hole, acting as a gravity-induced load on the surface of the hole. It can be presumed that the increased gravity force might have enhanced the sintering mechanisms, determining a higher dimensional change than expected. On the other hand, gravity could have determined the collapse of the hole structure, sharpening the elliptical section, and consequently the underestimation of the sintered diameter by least squares method.

The dimensional change of diameter in samples 0°, instead, is in principle unaffected by the gravity force, and in fact the trend is opposite with respect to sample 90°: in this case the dimensional change of diameter tends to increase on increasing the diameter size. The trend could be ascribed to an inhomogeneous densification on sintering, which in turn derives from an inhomogeneous heating rate of the sample. During sintering the heat is transmitted from the surfaces to the inner body by thermal conduction. In samples 0° the material surrounding the surface of the hole significantly decreases on increasing the diameter size, so that it reasonably heats up faster than the material surrounding smaller holes, consequently determining higher densification and dimensional change of larger holes.

In order to support this hypothesis, the dimensional change of the distance between axes of the holes is reported in Figure 9. In samples 0° the shrinkage of the distance between axes increases on considering

larger holes, according to the hypothesis of inhomogeneous heating rate on sintering and consequent larger shrinkage of bigger holes. The trend is generally confirmed in samples 30°, 45°, 60°, and less evident in 90° samples, where the inhomogeneity in heating rate is likely less pronounced due to the orientation. Further work is needed to quantitatively measure the local heating rates in different positions of the volume, aiming at validating the hypothesis above presented, and modeling the dimensional change accordingly. In fact, the surface to volume ratio controlling the thermal conduction is different for each sample. Moreover, the influence of gravity force has also to be considered in samples 30°, 45°, 60°, as previously in samples 90°.

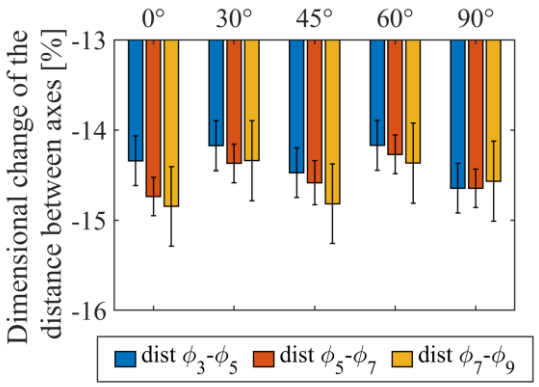

Figure 9. Dimensional change of the distance between axes of the holes in different geometries.

3.3 Variation in cylindricity

Figure 10 shows the cylindricity error derived from the measurement of holes in the samples in the green state. Irrespective on diameter size, the highest cylindricity error is observed for holes in samples 45°, and the lowest for holes in samples 90°.

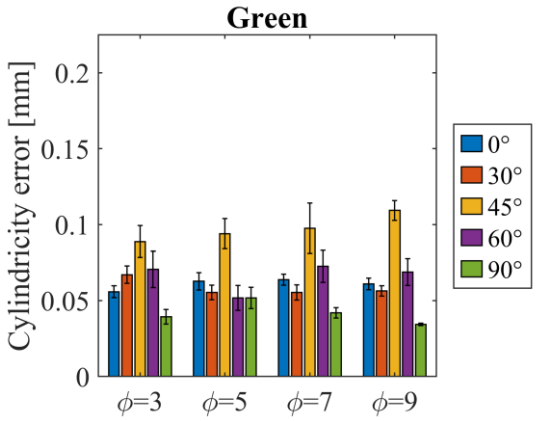

Figure 10. Cylindricity error of the holes in the green state.

Paul and Anand proposed a model for predicting cylindricity error as function of the staircase effect associated to layer by layer fabrication in additive manufacturing processes [20]. In the cited model, cylindricity error is a function of the building angle and has a parabolic trend: cylindricity error is zero at 0° and 180°, and shows the maximum, equal to layer thickness, at 90°. The trend proposed by Anand's geometrical model is in contrast with the experimental results of the present study, which highlights the effects of other process parameters than the layer-by-layer construction. In Dahmen et al, highest cylindricity has been observed corresponding to 45 degrees inclination [37]. According to Huang, cylindricity error is in fact affected by model, AM processing parameters (layer by layer construction is just one of them), and machine parameters [38].

Aiming at further investigating cylindricity error, Figure 11 shows the nominal geometry of one sample 0° in the reference system of the printing area, along with the position of the points measured on the planes parallel to Y-Z plane (blue dots), and the center of the circles derived from measurement at different levels on the surface of the holes (colored crosses).

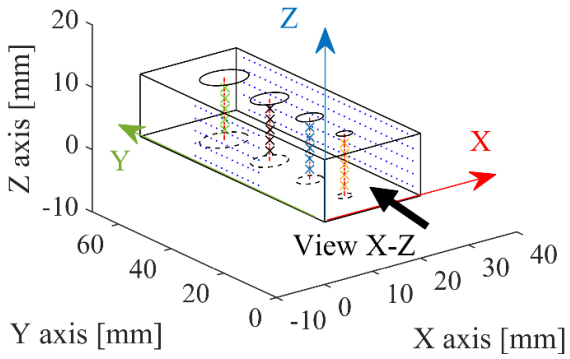

Figure 11. Nominal geometry of one sample 0° along with the points measured on the opposite planes parallel to Y-Z plane (blue dots), and the center of the circles derived from measurement at different levels on the surface of the holes (colored crosses).

Figure 12 reports the nominal geometry and measured points displayed in Figure 11, viewed by a direction orthogonal to X-Z plane, as indicated by the arrow, and projected on planes parallel to X-Z plane. Figure 12 reports the projections corresponding to three different X coordinates: left and right plots show the projection of the measured points on the planes parallel to Y-Z plane, and the projected position of the measured points (blue) is referred to the nominal position of the corresponding edge (0 mm and 20 mm on X axis, respectively). The central plot shows the projection of the center of the circles at different levels, again referred to the nominal position (10 mm on X axis). The measured points clearly deviate from nominal position, and in particular the maximum distance between the centers of the circles corresponds to the cylindricity error reported in Figure 10 for sample 0°. Same trend is observed in the other two samples °0. The influence of building parameters on the geometrical characteristics of parts produced by BJ is currently under investigation. As an example Rishmawi et al observed that deactivating roller determined a more evident layer shifting on green parts [36].
Aiming at improving the geometrical accuracy of the green parts, evidently affected by the building parameters, further study will investigate the control of printhead and roller movement, and the printing speed, in order to highlight the influence of the different parameters on the geometrical accuracy of the green parts.

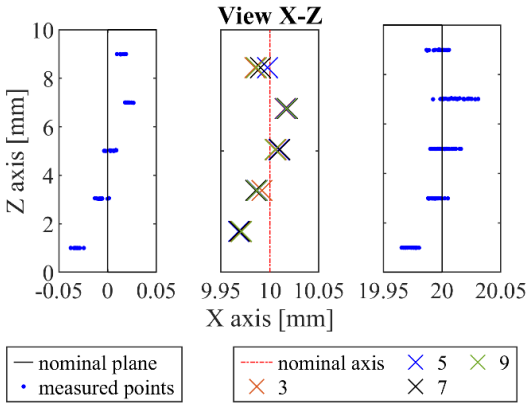

Figure 12. X-Z view of one sample 0° as by the arrow in Figure 11. The three plots show the magnification close to the nominal edges and the nominal axis of the hole, along with the projected points measured on the planes (blue dots) and the reconstructed center of circles at different levels (colored crosses).

The sintering process determined a worsening of cylindricity, as expected considering the anisotropic dimensional change (see Figure 13). In samples 0°, cylindricity error is about the same in green and sintered parts, since the dimensional change is isotropic in X-Y plane. On the other hand, on inclining the axis, the higher dimensional change in Z direction contributes to the form error, determining the increase in cylindricity error.

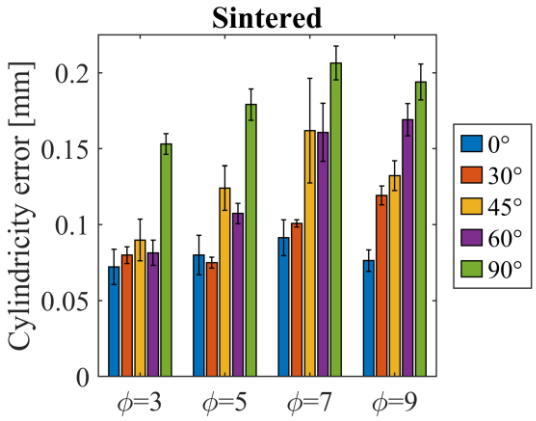

Figure 13. Cylindricity error of the holes in the sintered state.

The theoretical model previously described provides an analytical formulation of the cylindricity as function of the nominal diameter and inclination angle of the axis of the hole. Assuming the linear shrinkages, referred to the reference system of the printing area, equal to the mean values derived from measurement (see Table 4), equation (23) provides an estimation of the cylindricity error, displayed in Figure 14 by continuous lines (the different colors correspond to the different nominal size of diameters). The experimental results are shown as symbols, connected by dashed lines to highlight the trend.

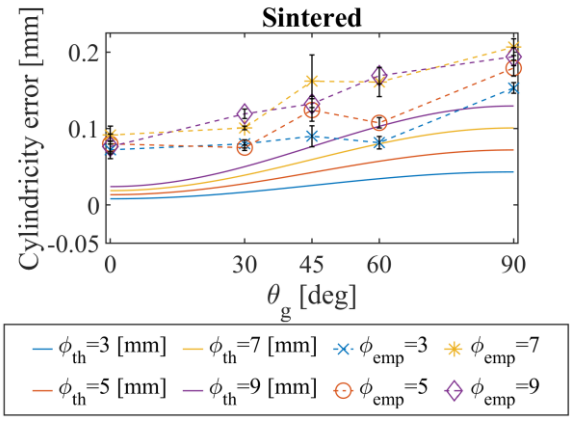

Figure 14. Cylindricity error predicted by the analytical model (continuous line) and derived from measurements of the sintered samples (symbols) versus the inclination angle.

Figure 14 shows that the cylindricity error is generally underestimated by the theoretical model. This is mainly due to the geometry of the real part that, as previously highlighted, is not perfectly corresponding to the nominal one, which is the reference for the theoretical model. Cylindricity of the holes in the green state is almost totally to be ascribed to the building parameters, so that considering the difference between cylindricity error in the sintered and in the green state, data are “cleaned” with respect to the building parameters, and actually represent the effect of sintering on cylindricity. Such difference is plotted in Figure 15 versus the inclination angle, along with the cylindricity error of the sintered parts, as predicted by the model.

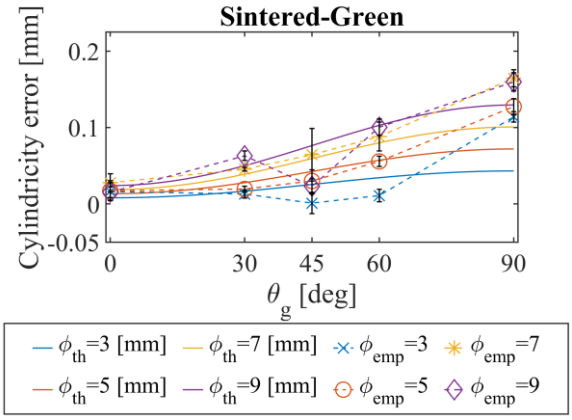

Figure 15. Cylindricity error predicted by the analytical model (continuous line) and derived from measurements as difference between the cylindricity error of sintered and green parts (symbols) versus the inclination angle.

Figure 15 reveals a significant improvement in the agreement between measured and predicted data, except for sample 45°, which deserves further investigation. The cylindricity error in sintered parts is confirmed to be directly related to the anisotropic dimensional change on sintering, and is effectively predicted by the analytical model, provided that the geometry of the part in the green state is close to the nominal one. Further study will be aimed at investigating the causes for the remaining discrepancies, mainly with relationship to the smallest holes. Again, the gradient in heating rate might play a significant role.

3.4 Variation in the inclination angle

Due to the anisotropic dimensional change on sintering, the angle of the axes of the holes is expected to slightly modify, according to equation (14), where the linear shrinkages are set equal to the mean values derived from measurement (see Table 4). Figure 16 shows the expected variation as a continuous line, along with the measured variation, represented by the colored symbols.

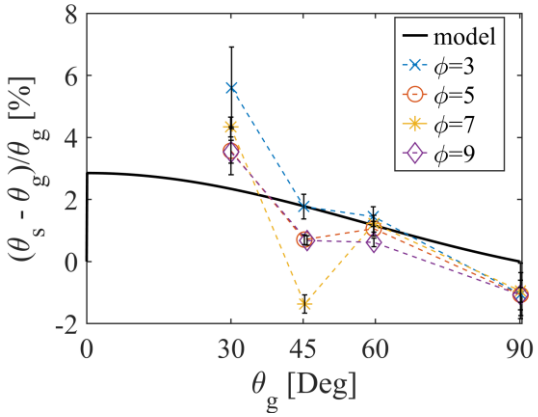

Figure 16. Normalized difference between sintered and green angle of the holes axes as function of the of the green angle – Expected variation (continuous line) along with measured variation (colored symbols).

Concerning the model, the inclination of the holes axes is affected by the anisotropy of dimensional changes, as shown in Figure 16, and the trend is confirmed by the experimental data. Nevertheless, the experimental data are not precisely matched by the model, which underestimates the angle deviation in sample 30° and

overestimates the angle deviation in samples 45° and, less significantly, 60°. Again, this is mainly due to the geometry of the real part in the green state. As previously highlighted, it is not perfectly corresponding to the nominal one, which is taken as the reference for the theoretical model. The inclination of the hole axes in the green parts, in fact, is not exactly corresponding to the nominal one, as highlighted in Figure 17.

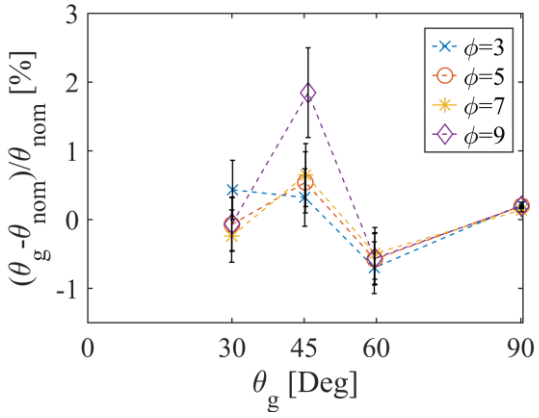

Figure 17. Normalized difference between green and nominal angle of the holes axes as function of the of the green angle.

The largest difference is observed in the sample 45°, as previously highlighted for cylindricity. Moreover, as for cylindricity, the difference between real and nominal angle in the green state does not improve the correspondence between real and predicted data in the sintered state, as it is instead observed for samples 30° and 60°. Further work will investigate the trend in sample 45°.

4. Conclusions

The dimensional and geometrical precision of AISI 316L samples produced by the binder jetting process was investigated in this work. The work is focused on the dimensional and geometrical characteristics of the four types of through holes, as affected by the size and axis inclination. The samples were measured in the green and sintered state, and the dimensional changes, as well as the variation in shape, were derived. An analytical model describing the dimensional change on sintering due to the anisotropy of the phenomenon was developed, and the expected dimensional changes and variations were compared to the measured ones.

The main results are summarized as follows:

- The analytical model can effectively predict the shrinkage of diameters. Slight discrepancies between predicted and measured data concern the smallest holes, and might be ascribed to the inhomogeneous heating rate and the consequent inhomogeneous densification on sintering (sample 0°) and to the gravity force effect (sample 90°).
- The analytical model underestimates the cylindricity error of sintered holes, and this is mainly due to the geometry of the real part, not perfectly corresponding to the nominal one, which is taken as the reference for the theoretical model. This hypothesis is demonstrated since the difference between sintered and green cylindricity error appreciably overlaps the predicted cylindricity error.
- The analytical model shows a moderate agreement with experimental data considering the variation in the inclination of the hole axes. As for cylindricity, this is supposed to be mainly due to the geometry of the real parts.

Dimensional changes and form variations are determined by both printing procedure and anisotropic shrinkage on sintering. The influence of anisotropic dimensional change on sintering can be effectively predicted by the proposed model.

Further work will be aimed at optimizing the printing parameters, also highlighting technical limits, if any, with respect to the matching between nominal and real geometry of the green parts. The model will be updated on the basis of the next experimentation, aiming at further improving the effectiveness and defining a useful tool for designers.

Acknowledgements

Authors would like to acknowledge the "Functional Sintered Materials (Funtasma)" Interdepartmental Laboratory of Politecnico di Milano, where this research activity was partially developed.
Support by the Italian Ministry for Education, University and Research through the project Department of Excellence LIS4.0 (Integrated Laboratory for Lightweight e Smart Structures) is also acknowledged.

References

[1] ASTM-F2792-12A, Standard Terminology for Additive Manufacturing Technologies, ASTM Int. (2012) 5–7. https://doi.org/10.1520/F2792-12A.2.

[2] M. Ziaee, N.B. Crane, Binder jetting: A review of process, materials, and methods, Addit. Manuf. 28 (2019) 781–801. https://doi.org/10.1016/j.addma.2019.05.031.

[3] M. Li, W. Du, A. Elwany, Z. Pei, C. Ma, Metal Binder Jetting Additive Manufacturing: A Literature Review, J. Manuf. Sci. Eng. 142 (2020) 1–17. https://doi.org/10.1115/1.4047430.

[4] A. Lores, N. Azurmendi, I. Agote, E. Zuza, A review on recent developments in binder jetting metal additive manufacturing: materials and process characteristics, Powder Metall. 62 (2019) 267–296. https://doi.org/10.1080/00325899.2019.1669299.

[5] S. Mirzababaei, S. Pasebani, A review on binder jet additive manufacturing of 316L stainless steel, J. Manuf. Mater. Process. 3 (2019) 8–12. https://doi.org/10.3390/jmmp3030082.

[6] Y. Bai, G. Wagner, C.B. Williams, Effect of particle size distribution on powder packing and sintering in binder jetting additive manufacturing of metals, J. Manuf. Sci. Eng. Trans. ASME. 139 (2017) 1–15. https://doi.org/10.1115/1.4036640.

[7] A. Mostafaei, P. Rodriguez De Vecchis, I. Nettleship, M. Chmielus, Effect of powder size distribution on densification and microstructural evolution of binder-jet 3D-printed alloy 625, Mater. Des. 162 (2019) 375–383. https://doi.org/10.1016/j.matdes.2018.11.051.

[8] B. Barthel, S.B. Hein, C. Aumund-Kopp, F. Petzoldt, Influence of Particle Size Distribution in Metal Binder Jetting – Effects on the Properties of Green and Sintered Parts, Proc. EuroPM2019, Int. Powder Metall. Congr. Exhib. (2019).

[9] M. Kafara, J. Kemnitzer, H.H. Westermann, R. Steinhilper, Influence of Binder Quantity on Dimensional Accuracy and Resilience in 3D-Printing, Procedia Manuf. 21 (2018) 638–646. https://doi.org/10.1016/j.promfg.2018.02.166.

[10] N.B. Crane, Impact of part thickness and drying conditions on saturation limits in binder jet additive manufacturing, Addit. Manuf. 33 (2020). https://doi.org/10.1016/j.addma.2020.101127.

[11] H. Chen, Y.F. Zhao, Process parameters optimization for improving surface quality and manufacturing accuracy of binder jetting additive manufacturing process, Rapid Prototyp. J. 22

(2016) 527–538. https://doi.org/10.1108/RPJ-11-2014-0149.

[12] Y. Wang, Y.F. Zhao, Investigation of Sintering Shrinkage in Binder Jetting Additive Manufacturing Process, Procedia Manuf. 10 (2017) 779–790. https://doi.org/10.1016/j.promfg.2017.07.077.

[13] A. Kumar, Y. Bai, A. Eklund, C.B. Williams, Effects of Hot Isostatic Pressing on Copper Parts Fabricated via Binder Jetting, Procedia Manuf. 10 (2017) 935–944. https://doi.org/10.1016/j.promfg.2017.07.084.

[14] H. Miyanaji, K.M. Rahman, M. Da, C.B. Williams, Effect of fine powder particles on quality of binder jetting parts, Addit. Manuf. 36 (2020). https://doi.org/10.1016/j.addma.2020.101587.

[15] L. Sun, Y.H. Kim, D. Kim, P. Kwon, Densification and properties of 420 stainless steel produced by three-dimensional printing with addition of Si3N4 powder, J. Manuf. Sci. Eng. Trans. ASME. 131 (2009) 0610011–0610017. https://doi.org/10.1115/1.4000335.

[16] T. Do, P. Kwon, C.S. Shin, Process development toward full-density stainless steel parts with binder jetting printing, Int. J. Mach. Tools Manuf. 121 (2017) 50–60. https://doi.org/10.1016/j.ijmachtools.2017.04.006.

[17] L. Rebaioli, I. Fassi, A review on benchmark artifacts for evaluating the geometrical performance of additive manufacturing processes, Int. J. Adv. Manuf. Technol. 93 (2017) 2571–2598. https://doi.org/10.1007/s00170-017-0570-0.

[18] F. Vitolo, M. Martorelli, S. Gerbino, S. Patalano, A. Lanzotti, Controlling form errors in 3D printed models associated to size and position on the working plane, Int. J. Interact. Des. Manuf. 12 (2018) 969–977. https://doi.org/10.1007/s12008-017-0441-9.

[19] R. Arni, S.K. Gupta, Manufacturability analysis of flatness tolerances in solid freeform fabrication, J. Mech. Des. Trans. ASME. 123 (2001) 148–156. https://doi.org/10.1115/1.1326439.

[20] R. Paul, S. Anand, Optimal part orientation in Rapid Manufacturing process for achieving geometric tolerances, J. Manuf. Syst. 30 (2011) 214–222. https://doi.org/10.1016/j.jmsy.2011.07.010.

[21] I.H. Ahn, S.K. Moon, G. Bi, Hole design quality identification in laser aided additive manufacturing, Proc. Inst. Mech. Eng. Part B J. Eng. Manuf. 232 (2018) 909–917. https://doi.org/10.1177/0954405416657584.

[22] R. Paul, S. Anand, Optimization of layered manufacturing process for reducing form errors with minimal support structures, J. Manuf. Syst. 36 (2015) 231–243. https://doi.org/10.1016/j.jmsy.2014.06.014.

[23] M.N. Islam, S. Sacks, An experimental investigation into the dimensional error of powder-binder three-dimensional printing, Int. J. Adv. Manuf. Technol. 82 (2016) 1371–1380. https://doi.org/10.1007/s00170-015-7482-7.

[24] T. Ollison, K. Berisso, Three-dimensional printing build variables that impact cylindricity, J. Ind. Technol. 26 (2010) 1–10.

[25] A. Farzadi, M. Solati-hashjin, M. Asadi-eydivand, N. Azuan, A. Osman, Effect of Layer Thickness and Printing Orientation on Mechanical Properties and Dimensional Accuracy of 3D Printed Porous Samples for Bone Tissue Engineering, 9 (2014) 1–14. https://doi.org/10.1371/journal.pone.0108252.

[26] I. Cristofolini, C. Menapace, M. Cazzolli, A. Rao, W. Pahl, A. Molinari, The effect of anisotropic dimensional change on the precision of steel parts produced by powder metallurgy, J. Mater. Process. Technol. 212 (2012) 1513–1519. https://doi.org/10.1016/j.jmatprotec.2012.02.009.

[27] I. Cristofolini, N. Corsentino, A. Molinari, M. Larsson, Study of the influence of material and geometry on the anisotropy of dimensional change on sintering of Powder Metallurgy parts, Int. J.

Precis. Eng. Manuf. 15 (2014) 1865–1873. https://doi.org/10.1007/s12541-014-0540-5.

[28] A. Molinari, S. Amirabdollahian, M. Zago, M. Larsson, I. Cristofolini, Effect of geometry and green density on the anisotropic sintering shrinkage of axisymmetric iron parts, Powder Metall. 61 (2018) 267–275. https://doi.org/10.1080/00325899.2018.1483064.

[29] M. Zago, I. Cristofolini, A. Molinari, New interpretation for the origin of the anisotropic sintering shrinkage of AISI 316L rings based on the anisotropic stress field occurred on uniaxial cold compaction, Powder Metall. 62 (2019) 115–123. https://doi.org/10.1080/00325899.2019.1601378.

[30] A. Molinari, M. Zago, S. Amirabdollahian, I. Cristofolini, M. Larsson, Anisotropic sintering shrinkage of ring shaped iron parts: Effect of geometry and green density and correlation to the stress field during uniaxial cold compaction, Proc. EuroPM2017, Int. Powder Metall. Congr. Exhib. (2017).

[31] M. Mariani, R. Beltrami, F. Meneghetti, D. Azzolini, N. Lecis, Effect of printing parameters on the mechanical strength of green body from binder jetting additive manufacturing, Proc. EuroPM2020, Int. Powder Metall. Virtual Congr. Exhib. (2020).

[32] ISO-14638:2015, Geometrical product specifications (GPS) — Matrix model, (2015) 16. https://www.iso.org/standard/57054.html.

[33] Y. Zhu, Z. Wu, W.D. Hartley, J.M. Sietins, C.B. Williams, H.Z. Yu, Unraveling pore evolution in post-processing of binder jetting materials: X-ray computed tomography, computer vision, and machine learning, Addit. Manuf. 34 (2020) 101183. https://doi.org/10.1016/j.addma.2020.101183.

[34] E.A. Olevsky, R.M. German, Effect of gravity on dimensional change during sintering - I. Shrinkage anisotropy, Acta Mater. 48 (2000) 1153–1166. https://doi.org/10.1016/S1359-6454(99)00368-7.

[35] E.A. Olevsky, R.M. German, A. Upadhyaya, Effect of gravity on dimensional change during sintering - II. Shape distortion, Acta Mater. 48 (2000) 1167–1180. https://doi.org/10.1016/S1359-6454(99)00369-9.

[36] I. Rishmawi, M. Salarian, M. Vlasea, Tailoring green and sintered density of pure iron parts using binder jetting additive manufacturing, Addit. Manuf. 24 (2018) 508–520. https://doi.org/10.1016/j.addma.2018.10.015.

[37] T. Dahmen, C.G. Klingaa, S. Baier-Stegmaier, A. Lapina, D.B. Pedersen, J.H. Hattel, Characterization of channels made by laser powder bed fusion and binder jetting using X-ray CT and image analysis, Addit. Manuf. 36 (2020) 101445. https://doi.org/10.1016/j.addma.2020.101445.

[38] Z. Huang, J.Y. Dantan, A. Etienne, M. Rivette, N. Bonnet, Geometrical deviation identification and prediction method for additive manufacturing, Rapid Prototyp. J. 24 (2018) 1524–1538. https://doi.org/10.1108/RPJ-07-2017-0137.